

# Research and Development Trends of Stainless Steel and Its Future Prospects

Masayuki ABE\*

## Abstract

*For the past decade, we have been developing environmentally friendly and resource-saving products. As a result, research and development to replace general-purpose stainless steel, expand demand for existing products, and meet new demand has progressed. In order to develop stainless steel that meets the needs of society in the future, it is important to develop microstructure control technology that produces more features and solution technology for customers. This paper outlines the trends in research and development to date and prospects for future efforts.*

## 1. Introduction

Japan started to use stainless steel in home and commercial equipment by making the most of its excellent properties like corrosion resistance and surface aesthetics in the 1960s. The demand for stainless steel increased for industrial equipment like oil plants and for construction and transport equipment in the 1970s. In the 1990s, stainless steel was used in automobile exhaust system parts, among other applications. Stainless steel production has increased to meet the social needs of the times.

At present, Japan's production of stainless steel is slightly below 3 million tons. The global production of stainless steel has grown from 30 million tons to about 60 million tons annually over the last 10 years due to the growth of stainless steel production in Asia and mainly China. Under such intensifying global competition, Nippon Steel Stainless Steel Corporation has worked to develop resource-saving stainless steel to substitute for general-purpose stainless steel, and has made efforts to maintain its competitiveness. We have taken initiatives to expand the demand for stainless steel and have carried out the development of manufacturing technology and solution technology to support the development of new applications and products.

The real thrill of advancing the research and development of stainless steel is to fully exploit the principal element Cr, the ferrite forming elements Si, Mo, Al, Nb, Ti, and Sn, and the austenite forming elements Ni, Cu, Mn, C, and N by combining these constituent elements in the best possible ways. Microstructurally, many matrix microstructures such as ferrite microstructure, austenite microstructure, ferrite-austenite duplex microstructure, and martensite microstructure due to strain-induced transformation are selectively

used and combined with precipitates to develop the metallurgy for stainless steel to display corrosion resistance, heat resistance, and other unique properties in specific applications. In this paper, we describe the stainless steel research and development trends, mainly conducted by Nippon Steel Stainless Steel over the past 10 years, and future prospects for stainless steel.

## 2. Product Development and Metallurgy to Meet Social Needs

### 2.1 Product development to replace general-purpose stainless steel

The most common stainless steels are austenitic SUS304 (18Cr-8Ni) and ferritic SUS430 (17Cr). We have carried out product development in pursuit of resource conservation and cost reduction while ensuring the corrosion resistance, the basic property of the SUS304 and SUS430.

#### 2.1.1 Development of lean duplex stainless steel capable of being welded with high heat input

The duplex stainless steel we studied as an alternative to the SUS304 contains about 50% each of the austenite phase and the ferrite phase, and its strength is high due to its fine grain size. It is characterized by a lower Ni content than in austenitic stainless steel. The conventional general-purpose duplex stainless steel S32101 (21.5Cr-5Mn-1.5Ni-0.4Mo-0.5Cu-0.22N) has the same base metal corrosion resistance as that of the SUS304 but its weld zone corrosion resistance is poorer. We improved the weld zone corrosion resistance of the S32101 to the same level as that of the SUS304 and developed the NSCC 2120™ (21Cr-2Ni-3Mn-1Cu-0.18N) by sup-

\* Executive Officer, Head of Research & Development Center, Research & Development Center, Nippon Steel Stainless Steel Corporation  
3434 Ooaza-shimata, Hikari City, Yamaguchi Pref. 743-8550

pressing the precipitation driving force of the Cr nitride responsible for the poor weld zone corrosion resistance.<sup>1)</sup> We also developed the NSSC™ 2351 (23Cr-5Ni-1Mo-Nb-0.18N) as a stainless steel that can substitute the SUS316L (17Cr-12Ni-2Mo) with higher corrosion resistance than that of the SUS304.<sup>2,3)</sup>

The conventional idea of inhibiting the precipitation of the Cr nitride mainly consisted of adding the inexpensive and austenite-forming element N in the largest soluble amount and utilizing the added N for the precipitation of the austenite phase during cooling.<sup>4)</sup> Thus, the austenite phase disappears or decreases in the heat-affected zone of the conventional duplex stainless steel at a temperature of about 1300°C. The N is expelled from the austenite phase and dissolved in the ferrite phase. During subsequent cooling, however, the solute N is not sufficiently redistributed in the austenite phase and precipitates as Cr nitride at the grain boundaries of ferrite. The corrosion resistance of the conventional duplex stainless steel consequently deteriorates in low-Cr regions around the Cr nitride.<sup>5)</sup>

The development of the NSSC 2120 revealed the importance of suppressing the precipitation of nitride not only in the ferrite phase but also in the regions heated to the ferrite-austenite phase through detailed observation of the weld heat-affected zone.<sup>6)</sup> As shown in Fig. 1, the formation of the austenite phase in the cooling process after heating to near the ferrite phase is ensured by optimizing Ni, Cu, N, Mn, etc., while suppressing the precipitation of the Cr nitride at 900°C or less.<sup>7)</sup> Specifically, the effects of Ni and N on the equilibrium precipitation temperature of the Cr nitride are clarified as shown in Fig. 2.<sup>1)</sup> The Cr nitride precipitation temperature is lowered by considering the effects of the respective alloying elements. Also, the N content is controlled to below 0.2% to shift the precipitation nose of the Cr nitride toward a longer period time and to secure the corrosion resistance.<sup>8)</sup> The composition design allows for manufacturability and alloy cost in addition to the above-mentioned improvement in corrosion resistance. This idea is also applied to the NSSC 2351.

### 2.1.2 Development of lean stainless steel utilizing Sn

To achieve resource conservation with the typical ferritic stainless steel SUS430, we studied the use of Sn as a means for securing the corrosion resistance while reducing the Cr content. We consequently developed the NSSC FW1 (14Cr-0.1Sn) with the same level of corrosion resistance as that of the SUS430. We also developed the NSSC FW2 (16Cr-0.2Sn) with even better corrosion resistance.<sup>9)</sup>

From the Pourbaix potential-pH diagram, we realized that Sn has a wide passive region as Cr does and contributes to the improvement of corrosion resistance.<sup>9)</sup> From the measurement of polariza-

tion curves in a 5% sulfuric acid solution as shown in Fig. 3, we clarified that the anodic dissolution peak of the 14Cr-0.1Sn steel is lower than that of the SUS430LX (17Cr-Ti-LC), namely that the 14Cr-0.1Sn steel is less susceptible to dissolution than the SUS430LX. We also found that the current density in the passive state region is equivalent to that for the SUS430LX,<sup>10)</sup> namely that the 14Cr-0.1Sn steel has good corrosion resistance.

From the investigation of the effect of Sn<sup>2+</sup> ions added to sulfuric acid, the corrosion rate decreased with the amount of Sn<sup>2+</sup> ions added, and the suppression of cathodic and anodic reactions were also confirmed, suggesting that the improvement in corrosion resistance was due to the adsorption of Sn<sup>2+</sup> ions.<sup>11)</sup>

We examined the existing state of Sn by performing surface analysis with hard X-ray photoelectron spectroscopy (HAXPES). We found that Sn exists mixed with the metal Sn, SnO<sub>2</sub>, and SnO is a transition process from the steel surface to the passive film. It was also found that an oxide film mainly composed of Cr grows in the atmospheric environment and that the formation of Sn oxide (SnO<sub>2</sub>) also progresses in the atmospheric environment.<sup>12)</sup> The state of Sn in the passive film is also being clarified in this way.

## 2.2 Research and development toward demand expansion

### 2.2.1 Initiatives in automotive field

In the automotive field, stainless steel is used mainly in exhaust system parts. We have conducted research and development in pursuit of the resource conservation and cost reduction of stainless steels for exhaust manifolds operating at 750 to 950°C and collecting the engine exhaust gas; flexible tubes operating at 600 to 800°C and arranged at the back of the exhaust manifolds to prevent the

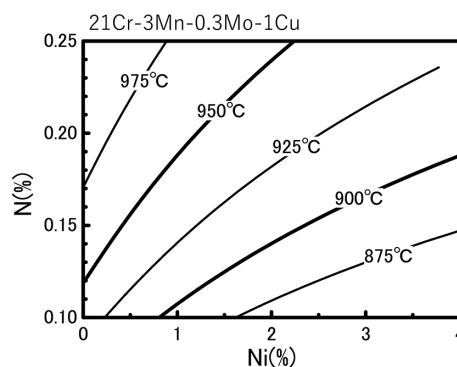


Fig. 2 Effect of Ni and N amounts on equilibrium precipitation temperature of Cr nitrides (Thermo-Calc calculation results)

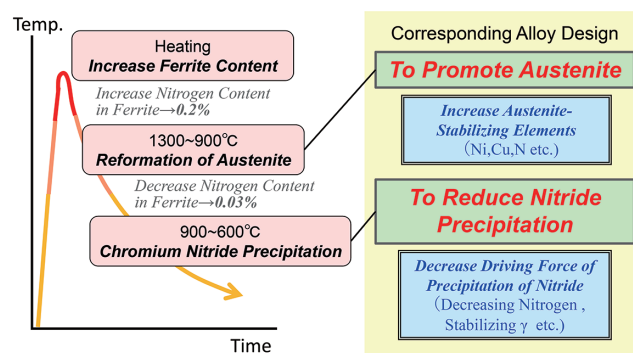


Fig. 1 Schematic diagram showing main phenomena occurring in heat-affected zone of duplex stainless steel in each cooling temperature range and alloy design to suppress their adverse effects

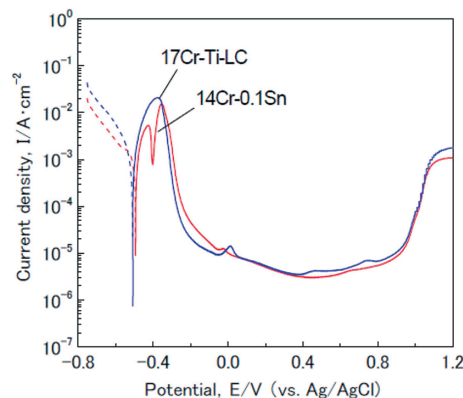


Fig. 3 Polarization curves of 14Cr-0.1Sn and 17Cr-Ti-LC stainless steels in 5% H<sub>2</sub>SO<sub>4</sub> solution at 30°C

transmission of the engine vibration to mufflers and exhaust pipes; and turbochargers increasingly mounted from a downsizing point of view.

(1) Development of stainless steel with excellent high-temperature strength for exhaust manifolds

Ferritic stainless steel with a small coefficient of thermal expansion was traditionally used for exhaust manifolds. Examples are the SUS429 (14Cr-1Si-Nb) microalloyed with Nb to ensure high-temperature strength and the SUS444 (19Cr-2Mo-Nb) microalloyed with Mo to provide high-temperature strength. To reduce the use of the expensive Nb and Mo, Cu precipitation strengthening was employed to improve the high-temperature strength at 600 to 800°C and to provide excellent thermal fatigue resistance. The results of our R&D efforts were the NSSC 429NF (14Cr-1.2Cu-0.1Ti), a SUS429 type and containing no Nb,<sup>13)</sup> the NSSC EM-C (17Cr-1.4Cu-0.55Nb-0.15Ti) with the Mo content reduced to impart resistance to exhaust gases of about 850°C,<sup>14)</sup> and the NSSC 448EM (17Cr-1.2Cu-0.3Mo-0.55Nb-0.1Ti).<sup>13)</sup> In the development of the NSSC EM-T (17Cr-0.8Mn-1.5Cu-2.0Mo-1.3W-0.5Nb) capable of resisting the exhaust gas at 950°C, a temperature exceeding the operating temperature of the SUS444, the most advanced of the existing stainless steels, its strengthening was achieved by utilizing Cu and optimizing Mo, W, and Nb.<sup>15)</sup>

The above Cu precipitation strengthening is strongly related to the thermal fatigue process. In static heat treatment, Cu particles having the KS orientation relationship with the matrix phase grow rodlike with time. In the state where tensile stress is applied, rod-shaped Cu precipitates decrease with the increase in strain. Fine spherical Cu precipitates with no increase in orientation relationships instead.<sup>16)</sup> In a thermal fatigue test involving thermal cycling close to that in actual usage, spherical Cu particles are observed as shown in Fig. 4. At 1 000 cycles or about one-third of the thermal fatigue life, many Cu particles are densely present, and many dislocations are entangled. Microstructural observation at 2 600 cycles at the end of the test recognized that the Cu particles are not coarsened. From the above, it is considered that the Cu particles can maintain a finely dispersed state and acquire the high-temperature strengthening capability by repeating strain-induced fragmentation, redissolution, and reprecipitation in the high-temperature deformation process.<sup>16)</sup>

(2) Development of stainless steel with excellent high-temperature salt damage resistance

Austenitic stainless steels such as SUS316L and SUSXM15J1 (19Cr-13Ni-3Si) are used for flexible tubes that require stringent workability. In areas where deicing salt is used in winter, high-temperature salt damage is likely to occur from the progress of corrosion by the deposited deicing salt. From the viewpoint of inhibiting corrosion, we investigated the effect of the composition on this high-temperature salt damage. We found that Si is effective in suppress-

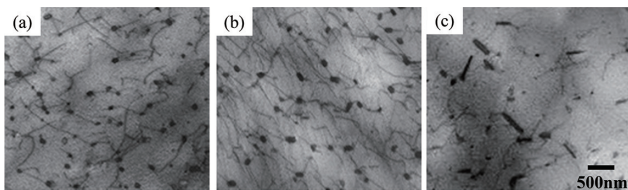


Fig. 4 TEM micrographs Cu precipitation in 14Cr-1.2Cu stainless steel after (a) 1 000 cycles and (b) 2 600 cycles with 50% restriction ratio in temperature range of 200°C to 700°C and after (c) heat treatment at 700°C for 87 h

ing uniform corrosion and that low C and Mo are effective in suppressing intergranular corrosion. We also clarified that a high Cr content is not effective against high-temperature salt damage. We subsequently developed the NSSC 307FX (17Cr-13Ni-3Si-1.5Mo-lowC) with both high-temperature strength and oxidation resistance.<sup>17)</sup>

Regarding the above-mentioned effect of Cr, we analyzed the corrosion products formed in the high-temperature combined cyclic corrosion test consisting of NaCl aqueous solution immersion cycles and heat treatment cycles in the atmosphere at 650°C or 700°C. We found that the test specimens are corroded in proportion to the Cr composition of the base metal as schematically illustrated in Fig. 5<sup>18)</sup> and that the Cr film is not stable in the test environment. On the other hand, Si was not detected on the specimen surfaces and in the corrosion products in the NaCl aqueous solution. Si is thus considered to exist as a stable oxide at the interface between the base metal and the corrosion products<sup>18)</sup> and contributes to the improvement of corrosion resistance. Because Ni and Mo also corrode at a lower rate than the ratio of components in steel, Ni and Mo are judged to be effective for corrosion resistance<sup>18)</sup> and the above-mentioned composition design is adopted.

(3) Development of stainless steel with excellent high-temperature sliding properties

Turbochargers are used to improve the fuel efficiency of automobiles and are required to have a high-temperature slidability in addition to high-temperature strength. High-Ni heat-resistant steel like the SUS310S (25Cr-20Ni) is applied to the principal parts of nozzle vane turbochargers. We developed the NSSC LHT (19Cr-13Ni-3Si-0.1Nb-0.03C) with excellent high-temperature slidability and strength by utilizing Si-based oxides to reduce the Cr and Ni contents and to achieve resource conservation and cost reduction by microalloying with Nb to secure strength and by lowering the C content.<sup>19)</sup>

The improvement of the slidability with Si is considered due to the oxide morphology on the surface shown in Fig. 6. For the SUS304 and SUS310S with a Si content of about 0.4%, it is presumed as follows. Needle-like or angular oxides form on the sliding surface during high-temperature heating and increase the dynamic friction force in the initial stage of sliding. The oxides peel off in the sliding process, build up on the sliding surface, coarsely adhere to

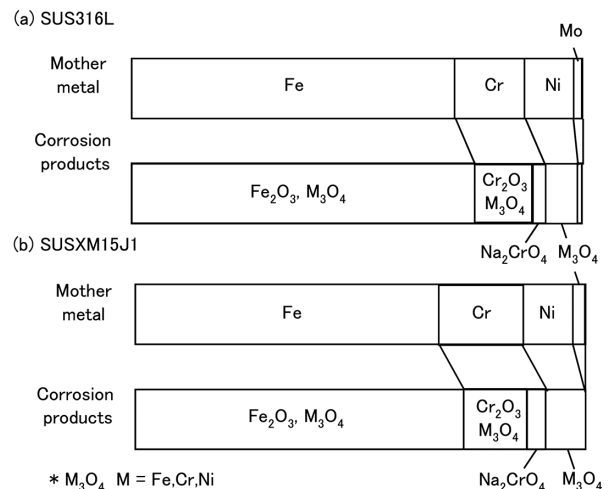


Fig. 5 Schematic composition diagram of corrosion products on SUS 316L and SUSXM15J1 after NaCl-induced hot corrosion tests



Fig. 6 SEM images of surface after heat treatment at 800°C for 1 hour in air

the sliding surface, and mar the sliding surface. It is thought that deposits and coarse adhesions on the surface lead to defects. With the NSSC LHT microalloyed with 3% Si, on the other hand, the sliding surface is covered with dense Si-based oxides during heating. Hence, the dynamic friction force is reduced, and the oxides peel off less during sliding. In addition, the high-temperature strength and the slidability are improved by microalloying with Nb.<sup>20)</sup>

### 2.2.2 Initiatives in home and commercial equipment field

#### (1) Stainless steel for hot water tanks and their corrosion resistance

The NSSC 190 (19Cr-2Mo-Nb, Ti) with excellent stress corrosion cracking resistance in a hot water environment of about 80°C was conventionally used for electric hot water tanks in home hot water supply systems. In recent years, new hot water supply systems with higher efficiency and energy conservation have been developed as described below, and the hot water tank materials have been optimized to adapt to these systems.

As for electric water heaters, natural refrigerant heat pump water heaters that use CO<sub>2</sub> as a refrigerant with one-third electricity consumption were developed. These new water heaters required Mo-saving materials to cope with the price rise in Mo. The corrosion resistance requirements were the inhibition of crevice corrosion in shell-to-end plate welds and the assurance of corrosion resistance in the heat-affected zones. Accordingly, we developed the NSSC 220ECO (22Cr-1.2Mo-Ti-Nb) with Mo substituted by Cr and, in addition, we applied the NSSC 445M2 (22Cr-1Mo-Ti-Nb) in this field.<sup>21, 22)</sup>

Latent heat recovery gas water heaters were also developed with a secondary heat exchanger to utilize the waste heat from the primary heat exchanger of the gas water heater. Recovery of the latent heat from the combustion exhaust gas of about 150°C results in the formation of condensed water with a pH of about 3 and containing SO<sub>4</sub><sup>2-</sup> and NO<sub>3</sub><sup>-</sup> derived from the combustion gas in the secondary heat exchanger. In addition, the infiltration of airborne salt creates a severe corrosive environment in the secondary heat exchanger. The SUS316L and similar materials were traditionally used in such secondary heat exchangers. In contrast, we studied the application of ferritic stainless steel with lower Ni and good thermal conductivity. We conducted laboratory tests simulating the severe corrosive environment described above and actual environment exposure tests. We accordingly clarified that the NSSC 220ECO can be used in that environment.<sup>22)</sup>

A fuel cell cogeneration system generates electricity by using hydrogen from the reforming of city gas and oxygen from the air, and is equipped with a hot water supply system to utilize the heat from electricity generation. The electricity generation system is a polymer electrolyte fuel cell (PEFC) or a solid oxide fuel cell (SOFC). The supplied hot water is low in temperature at about 65°C and the corrosive environment is mild. Given these conditions, we developed the NSSC 190ECO (19Cr-1Mo-Nb, Ti) by considering the corrosion resistance and cost in the applicable hot water environment, as well as the strength assurance and weld workability, by reducing the Mo content of the NSSC 190 and by microalloying with

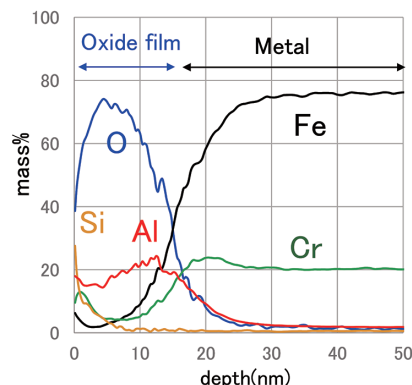


Fig. 7 Profile of elements from surface after bright annealing of 18Cr-2Al stainless steel

both Nb and Ti.<sup>22)</sup>

#### (2) Development of stainless steel for SOFC

The operating environment of the SOFC during electricity generation contains water vapor and is at 700 to 1000°C. The Cr<sub>2</sub>O<sub>3</sub> film on the stainless steel surface reacts with the water vapor and oxygen to produce volatile CrO<sub>2</sub>(OH)<sub>2</sub>. Cr precipitates near the air electrode and reduces the electricity generation efficiency. Conventionally, stainless steel with an Al<sub>2</sub>O<sub>3</sub> film formed by microalloying with about 3% Al was used to suppress the Cr evaporation. We investigated the Al content reduction from the viewpoints of formability, resource conservation, and cost reduction. We accordingly found that a sound Al<sub>2</sub>O<sub>3</sub> film can be formed by proper microalloying with Nb, despite the Al content reduction, and successfully developed the NSSC NCA-F (18Cr-1.5Al-0.2Nb).<sup>23)</sup>

We are also investigating the process whereby an Al<sub>2</sub>O<sub>3</sub> film is formed as a result of Al microalloying. The element profiles of bright annealed 18Cr-2Al stainless steel specimens were measured with a glow discharge optical emission spectrometer (GDS). As shown in Fig. 7, the Fe and Cr concentrations significantly decreased about 15 nm from the surface and Al was the main constituent of the oxide film. Analysis by X-ray photoelectron spectroscopy (XPS) revealed that the Al was trivalent Al<sub>2</sub>O<sub>3</sub> in the chemically bonded state. We have thus clarified the microstructure and formation process of Al<sub>2</sub>O<sub>3</sub>.<sup>24)</sup>

### 2.2.3 Initiatives in industrial equipment field

#### (1) Development of high-strength spring wire rod steel

Utilizing the strain-induced transformation of austenitic stainless steel, we have developed the Type SUS201 (17Cr-4.5Ni-4.5Mn-0.06C-0.18N) with a strength exceeding 2500 MPa. This is the highest strength among the stainless steel wire rods for high-strength springs. We consider that this strength of about 2000 MPa was achieved by a combination of component optimization for stable processing-induced transformation and 50% of the amount of martensite by cold working. In addition, we think that the strengthening was accomplished by utilizing the interaction of the N and dislocations in the strain-induced martensite and the austenite formed by aging at 200 to 500°C.<sup>25)</sup>

By applying the above idea to duplex stainless steel, we are also studying high-strength wire rods of the NSSC 2120 with a strength of 1800 MPa. Particularly, NSSC 2120 has a duplex structure with high N content (0.3%) in the austenite phase, so that in addition to the strain-induced martensite, supersaturated N and aging products provide a modulus of elasticity of about 85 GPa, higher than that of the commercial piano wire steel SWP-B.<sup>26)</sup> This characteristic is ex-

pected to contribute to the weight reduction of stainless steel coil springs.

**2.3 Research and development toward creation of new demands**

**2.3.1 Development of stainless steel for high-pressure hydrogen**

As initiatives to utilize hydrogen for CO<sub>2</sub> emission reduction and decarbonization, fuel cell vehicles are being deployed and hydrogen filling stations are being built.<sup>27)</sup> The hydrogen used in these applications is under high pressure. The SUS316L is standardized by law as hydrogen embrittlement resistant stainless steel in Japan. We developed the NSSC STH™1 (15Cr-9Mn-6Ni-Cu) with 600 MPa strength and with resource-saving and economical features by securing austenite phase stability by reducing the Cr, Ni, and Mo contents of the SUS316L and by utilizing the Mn and Cu. We also developed the NSSC STH2 (15Cr-9Mn-6Ni-Cu-0.2N) with 700 MPa strength, higher than that of the SUS316L, by microalloying with 0.2%.<sup>28, 29)</sup>

Hydrogen embrittlement may be (i) embrittlement by the martensite phase transformed by strain-induced transformation or (ii) embrittlement of the austenite phase containing various lattice defects due to plastic deformation.<sup>30)</sup> In the process of carrying out our research on the above-mentioned stainless steels for handling hydrogen, we obtained new findings about the embrittlement (ii). The SUS304 specimens charged with about 30 ppm of hydrogen were examined by synchrotron X-ray diffraction and a high-resolution transmission electron microscope (TEM) while being tensile strained. A nanosized ε phase was found to be formed on the twin interface as shown in Fig. 8.<sup>31)</sup> This ε phase is considered to have formed when dislocations accumulated at the austenite twin interface. The ε phase formed in the presence of hydrogen almost disappears at 400°C and is therefore considered to be a vacancy defect.<sup>32)</sup> In addition, we analyzed atomic vacancies and their clusters by positron annihilation spectroscopy that can detect them with high sensitivity. The analysis found that lattice defects formed by plastic deformation interact with hydrogen to stabilize vacancies and form

vacancy clusters in the SUS304. The stabilization of vacancies and the formation of vacancy clusters were shown to occur more actively than in the SUS316L.<sup>33)</sup> These findings advanced the elucidation of the mechanism whereby the vacancies in the ε phase cluster and form microvoids and the microvoids link up to cause the hydrogen embrittlement.

**2.3.2 Study of application of duplex stainless steel to infrastructure**

**(1) Application of duplex stainless steel to ozone environment**

Ozone has a high oxidizing power. When ozone is decomposed, it changes to oxygen and does not generate toxic substances as chlorination does. Ozone is thus used for sterilization, bleaching, deodorization, and other purposes. Because ozone has high oxidizability, the corrosion rate of copper and brass increases by increasing ozone concentration. On the other hand, SUS304 does not corrode.<sup>34)</sup> For this reason, the SUS304 and SUS316 are example materials for use in the ozone environment. We studied the NSSC 2120 with corrosion resistance equivalent to that of the SUS304 for use in the ozone environment. The NSSC 2120 demonstrated a corrosion resistance equivalent to that of the SUS304 in both the base metal and the weld zone in the ozone environment containing 200 ppm of Cl<sup>-</sup>, the upper limit of the Cl<sup>-</sup> concentration for tap water.<sup>35)</sup> It is now recognized as an example material.<sup>36)</sup>

When the surfaces of the SUS304 and SUS316L specimens exposed to wet ozone gas were investigated as related to the above discussion, the increase in the surface oxide film thickness and the improvement in the pitting potential were confirmed as compared with before the exposure.<sup>37)</sup> When the SUS304 specimens were immersed in ozone water, the surface film thickness tended to increase by ennoblement, and the formation of Fe and Cr oxide films was confirmed.<sup>38)</sup> It is speculated that the stable formation by the ozone of oxides on the surface contributes to the assurance of corrosion resistance.

**(2) Application of duplex stainless steel to building and civil engineering materials**

The NSSC 2120 is registered in the NETIS (New Technology Information System) of the Ministry of Land, Infrastructure, Transport and Tourism. Because it has high proof stress, it can be used to reduce the weight of equipment. In freshwater regions, it is adopted in the water intake equipment of dams.<sup>39)</sup> The NSSC 2351 is developed as a grade above the NSSC 2120 and is expected to be applied in environments where higher corrosion resistance is required.

We also studied the application of the NSSC 2120 wire rods to prestressed concrete. Prestressed concrete is concrete where compressive stress is applied beforehand by tendons like high-strength steel wire rods, which improves the tensile stress resistance, a weakness of conventional concrete and reinforced concrete. The NSSC 2120 wires strengthened to over 1400 MPa by cold drawing are confirmed to have characteristics equivalent to those of the SUS304 in environments where the threshold chloride ion concentration for corrosion initiation is 15 kg/m<sup>3</sup> for the SUS304 as described in the “Guidelines for Design and Construction of Concrete Structures Using Stainless Steel Reinforcement Bars (Draft)”.<sup>40)</sup> This indicates the applicability of duplex stainless steel in this field.

**3. Development of Manufacturing Technology and Solution Technology to Support Product Development**

To carry out product development as described above, it is equally important to develop manufacturing technology and utilization and fabrication technology. In terms of manufacturing, stainless

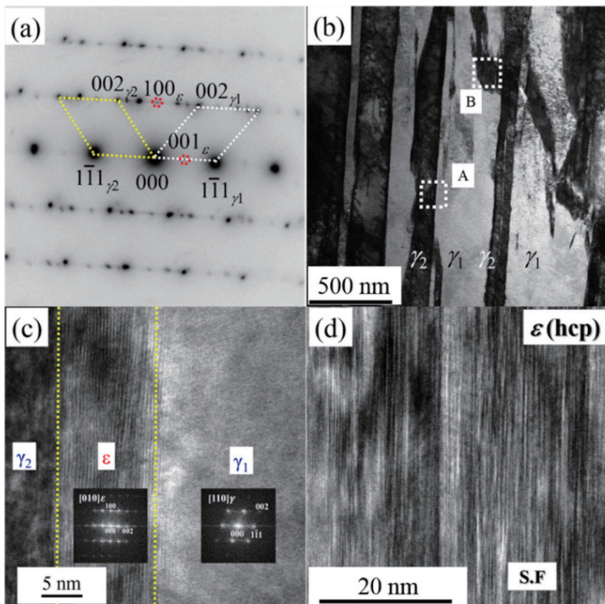


**Fig. 8 Observation of substructure of hydrogen embrittled SUS304**  
 (a) Electron diffraction pattern showing γ and ε phase (b) Dark-field image showing twin structure consisting of γ phase (c) High-resolution TEM image of ε phase in region A (d) High-resolution TEM image of ε phase with number of attacking faults in region B

steel does not have solid phase transformation like the austenite/ferrite transformation of carbon steel, and stainless steel is strongly affected by the solidification microstructure. In terms of utilization and fabrication, the high strength of stainless steel makes it difficult to fabricate stainless steel, and the joining technology of stainless steel is affected by alloying elements. We have worked to clarify and control these phenomena.

**3.1 Development of manufacturing technology to support product development**

**3.1.1 Development of solidification microstructure control technology**

(1) Study of solidification microstructure prediction technology by simulation

The solidification of stainless steel is roughly divided into: (i) F mode where the  $\delta$  ferrite single phase solidifies; (ii) FA mode where the ferrite phase solidifies first and the  $\delta$  ferrite phase then solidifies; (iii) AF mode where the austenite phase solidifies first and the  $\delta$  ferrite phase then solidifies; and (iv) A mode where the austenite single-phase solidifies. Even in the F mode, the austenite phases may precipitate during cooling after solidification as in duplex stainless steel. To clarify the solidification process and the subsequent microstructural change, we have studied the effects of alloying elements and the formation process of the second phase by utilizing the multi-phase field (MPF) method that has demonstrated its usefulness in recent years.

Concerning the SUS304 with the FA mode solidification, it is possible to simulate the dendrite growth of primary  $\delta$  ferrite, the

subsequent formation of the austenite phase between the dendrite arms, and the remainder of the  $\delta$  ferrite phase in a vermicular pattern with the growth of austenite.<sup>41)</sup> As shown in **Figs. 9** and **10**, we can now predict the microstructural change during reheating after solidification and the reduction behavior of residual  $\delta$  ferrite.<sup>42)</sup>

Regarding the solidification of high-alloy steel such as the 25Cr-15-19Ni-2Mo system in the AF mode and the subsequent microstructural change, the change of the ferrite phase to the intermetallic compound  $\sigma$  phase in the final solidification part where the alloying elements are concentrated can be analyzed by coordination with phase diagram calculation software. The application of the MPF method to the precipitate prediction has advanced in this way.<sup>43)</sup>

The morphology of the austenite phase that precipitates during cooling after solidification in the  $\delta$  ferrite phase in the F mode as in the case of duplex stainless steel can also be predicted in the 23Cr-6Ni-3Mo-0.1N system as shown in **Fig. 11**.<sup>44)</sup> The MPF method can also be applied to various solidification morphologies in stainless steel and microstructural changes during cooling. It is a useful technique for analyzing and predicting the solidification microstructure.

(2) Research of solidification microstructure refining technology

Surface defects like ridging and resulting from a coarse solidification microstructure occur in ferritic stainless steel that solidifies in F mode. To reduce ridging, many studies have been conducted on the grain refinement of the solidification microstructure. We have also focused on compositional supercooling and heterogeneous nucleation to refine the solidification microstructure and have studied the utilization of Ti and Mg based on the 16Cr stainless steel. When

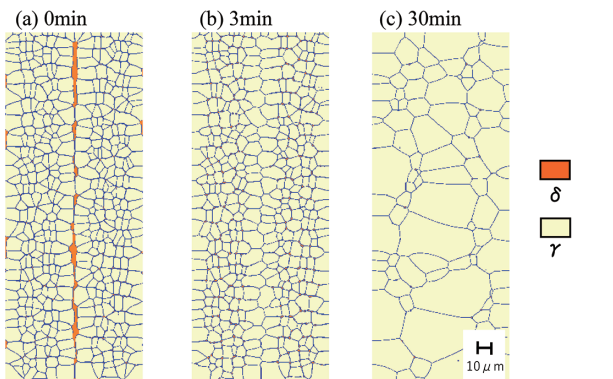


**Fig. 9** Distribution of phases during heat treatment at 1100°C, calculated by multi-phase field method

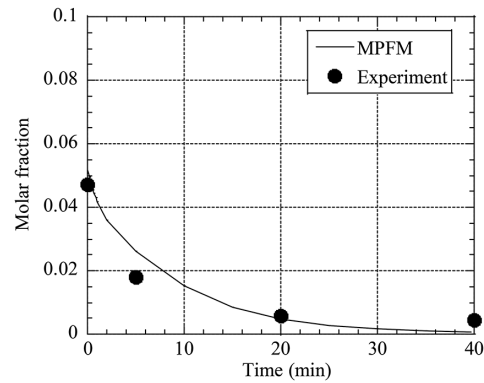


**Fig. 10** Dissolution behavior of  $\delta$  ferrite phase during annealing at 1100°C, calculated by MPF method and compared with experimental results

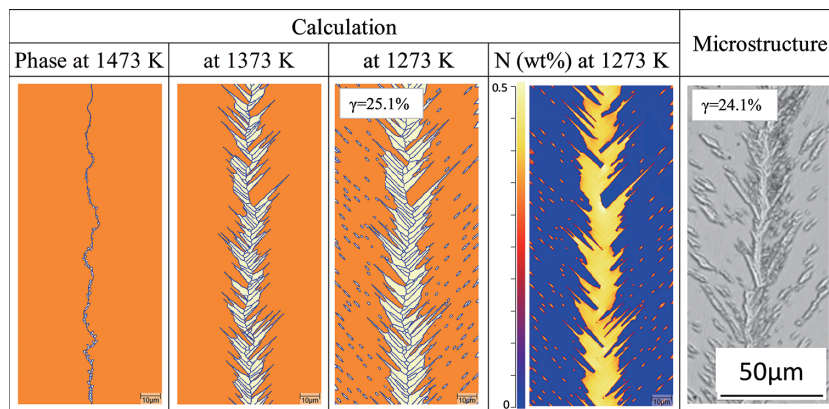


**Fig. 11** Calculation of  $\gamma$  phase precipitation behavior and N-distribution in duplex stainless steel by MPF method<sup>44)</sup>

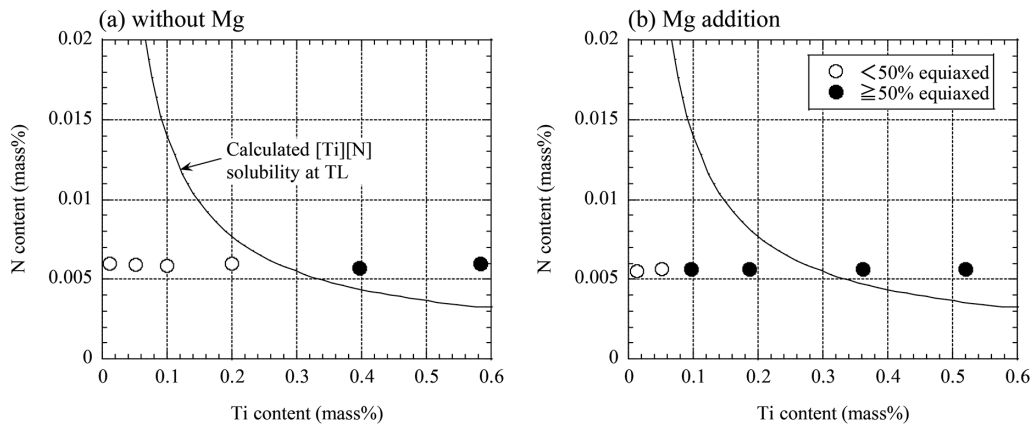


Fig. 12 Effect of Ti and Mg addition on equiaxed structure formation in 16Cr stainless steel

the additional content is small and the compositional supercooling is small, the columnar crystal width tends to narrow.<sup>45)</sup> When the Ti content is large as shown in Fig. 12, the compositional overcooling and heterogeneous nucleation by TiN facilitate the formation of equiaxed crystals. Furthermore, the addition of Mg was found to accelerate equiaxed crystallization. The Mg added as described above is considered to reduce Ti oxides, contribute to the formation of  $Al_2MgO_4$  and TiN, and promote the heterogeneous nucleation. When the Al concentration is high, equiaxed crystallization is inhibited. The importance of the relationship with deoxidation was thus clarified.<sup>46)</sup> The systematization of solidification microstructure control technology has progressed in this way.

3.1.2 Metallurgical research in hot and cold rolling processes

We have also applied the MPF method to the metallurgical phenomena related to the hot rolling process. Concerning the decomposition behavior of the austenite phase into the ferrite phase and Cr carbide during the annealing of hot-rolled SUS430 sheets, the resulting microstructure was predicted by the MPF method together with the integrated thermodynamic calculation software ThermoCalc. The MPF method has agreed well with experiments about the relationship between the precipitation morphology of Cr carbide and the temperature and about the time dependence of the Cr concentration.<sup>47)</sup> As noted above, the MPF method has proven its usefulness.

We have created the technology to predict the Lankford value ( $r$ -value), an index for drawing ferritic stainless steel, from its texture.<sup>48)</sup> As initiatives to improve the  $r$ -value, we have acquired guidelines for controlling the texture of ferritic stainless steel.<sup>49)</sup> For example, we have found that the higher the  $\{111\}$  orientation ratio in the microstructure before cold rolling, the more frequently  $\{111\}$  grains recrystallize from within the worked  $\{111\}$  grains in the annealing process after cold rolling. The initiatives to control the hot-rolled microstructure and to optimize subsequent manufacturing conditions are also underway.

3.1.3 Research on pickling efficiency

Stainless steel is commonly pickled by the electrolytic pickling process in which anode and cathode electrodes are placed in a pickling tank filled with an electrolytic aqueous solution containing sulfuric acid, for example, and a dissolution reaction is caused by indirect energization to descale the steel strip. We investigated the effect of the tank configuration on the electrolysis efficiency during sulfuric acid electrolysis in the electrolytic pickling process.<sup>50)</sup> We analyzed by simulation with the finite element method (FEM) the dissolution rate distribution in consideration of the reduction of the ef-

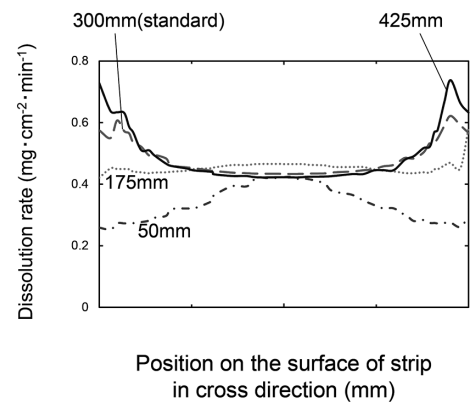


Fig. 13 Dissolution rate curve in central part of SUS430J1L strip simulated by FEM when changing width of cathode electrode

fective surface area due to the scale remaining on the strip surface. As shown in Fig. 13, the cathode electrode width is optimized when transpassive dissolution occurs.<sup>51)</sup> As noted above, we developed the simulation technology for the dissolution behavior during pickling.

3.2 Development of solution technology to support product development

It is also important to develop the solution technology to fully exploit the material properties of stainless steel. We have also tackled the development of press forming technology and welding technology mainly for the duplex stainless steels we have developed with massive efforts.

3.2.1 Development of press forming technology

One issue with the press forming of the NSSC 2120 sheet is that it has higher yield strength than the SUS304 and thus has a large springback. It is necessary to predict the springback to optimize the press forming die and improve formability. A comparison with actual press forming confirmed that the springback can be predicted by the Yoshida-Uemori model with high accuracy, as shown in Fig. 14. The tool clearance can be optimized.<sup>52)</sup> It was also found that the stop motion with a servo press in which a dwell time of about 0.5 s is taken at the bottom dead center can reduce the springback more than the crank motion.<sup>53)</sup> These findings are expected to be applied to technology development and actual part fabrication.

3.2.2 Development of joining technology

Metallurgical issues with joining stainless steel include welding cracks in austenitic stainless steel, austenitic phase precipitation behavior in duplex stainless steel, and brazability in ferritic stainless

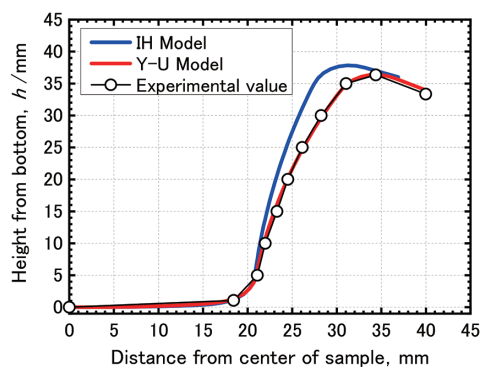


Fig. 14 Comparison of experiment and simulation on springback of NSSC 2120

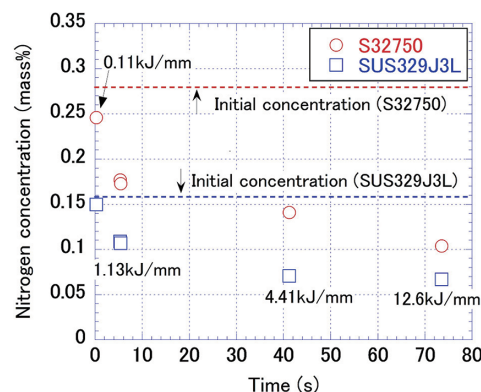


Fig. 16 Results of nitrogen desorption during welding of duplex stainless steel

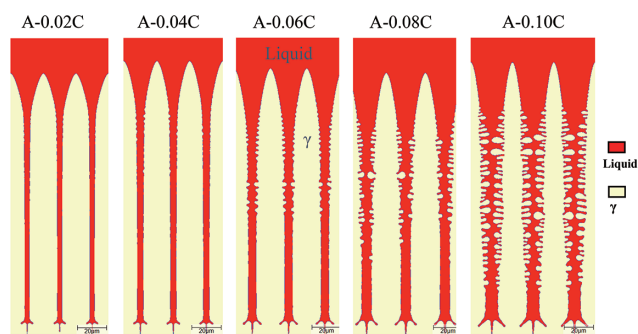


Fig. 15 Effect of C content on solidification microstructure calculated by MPF method (Fe-25%Cr-22%Ni-C alloy)

steels. We have worked to improve these problems.

(1) Research on weld cracking in austenitic stainless steel

Concerning weld cracking in austenitic stainless steel, we focused on the microstructural morphology during solidification and the solidification brittleness temperature range. With the MPF method, we can analyze the following: As the C content increases, the microstructural morphology transitions from cell to dendrite. As shown in Fig. 15, the transition to dendritic solidification occurs at a C content of 0.08% in the 25Cr-22Ni steel that solidifies in A mode. As the C content increases, the solidification brittleness temperature range increases to increase the cracking susceptibility.<sup>54)</sup> The effect of the N was also investigated by both experimentation and calculation. As the N content increases, the microstructure morphology transitions from cell to dendrite as in the case with the C content. The dendrite formation may suppress the enrichment of the Cr and P at the solidification interface.<sup>55)</sup> We have revealed these and other interesting microstructural behaviors.

(2) Research on microstructure formation in duplex stainless steel

It is important to understand the microstructure formation process of the austenite phase for welding duplex stainless steel. We experimented with the S32750 (25Cr-6.5Ni-3.5Mo-0.28N) and SUS 329J3L (22.5Cr-6Ni-3Mo-0.16N) by changing the heat input in argon-shielded TIG welding. As the heat input increases, the melting time increases as shown in Fig. 16, the N is released, and the N content decreases. It has also become clear that the precipitation temperature of the austenite phase becomes about 100°C lower than the equilibrium precipitation temperature, and the Widmanstätten-austenite phase grows with the K-S orientation relationship.<sup>56)</sup>

Laser welding has been increasingly applied in recent years, and the effects of the laser type (fiber or CO<sub>2</sub>) and the shielding gas type

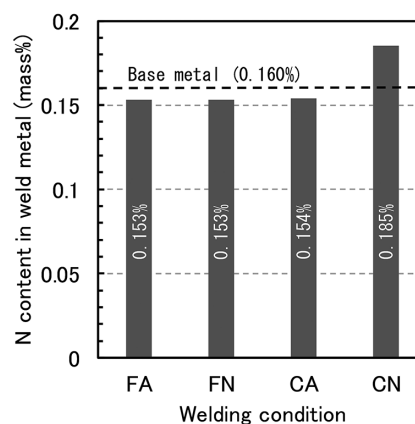


Fig. 17 Effect of laser type and shielding gas on nitrogen content of weld metal in laser weld (F: Fiber laser, C: CO<sub>2</sub> laser, A: Ar shield, N: N<sub>2</sub> shield)

(Ar or N<sub>2</sub>) are clarified for the NSSC 2120. Regardless of the laser type-shielding gas type combination, the pitting potential is about 0.3 V for the NSSC 2120 and is equivalent to that of the SUS304. With the combination CN of a long-wavelength CO<sub>2</sub> laser and N<sub>2</sub> atmosphere as shown in Fig. 17, the N pickup in the weld metal proceeds, the N content of the weld metal becomes higher than that of the base metal, and it was confirmed that the precipitation amount of the austenite phase is higher than that of the base metal. Concerning the precipitation behavior of the austenite phase, it is also confirmed that the austenite phase precipitates within the ferrite grains as well as at the ferrite grain boundaries to make the austenite phase higher than with any other combination.<sup>57)</sup> In this way, the combination of the welding method and the shielding gas is confirmed as another important factor for microstructure formation in duplex stainless steel.<sup>57)</sup>

(3) Research of brazing technology

Brazing is used for joining relatively small heat exchanger parts and automobile parts. We have investigated the effects of alloying elements on the brazing of ferritic stainless steel. Concerning the Nb and Ti used to stabilize the C and N, it has been found that the wettability and spreadability of Ni brazes during heat treatment at 1100°C for 30 min in an atmosphere with a dew point of -50°C are superior for Nb-microalloyed steel. As shown in Fig. 18, the oxide film thickness for the Nb-containing SUS444 is 5 nm and similar to that for the SUS316, and is more than 100 nm for the Ti-microalloyed SUS436L (18Cr-1Mo). It has become clear that it is also nec-

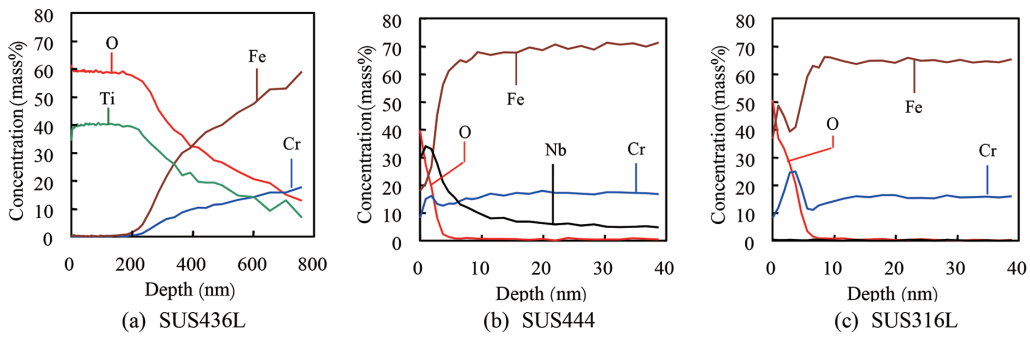


Fig. 18 Depth profile of oxide scale formed on specimens after brazing by XPS

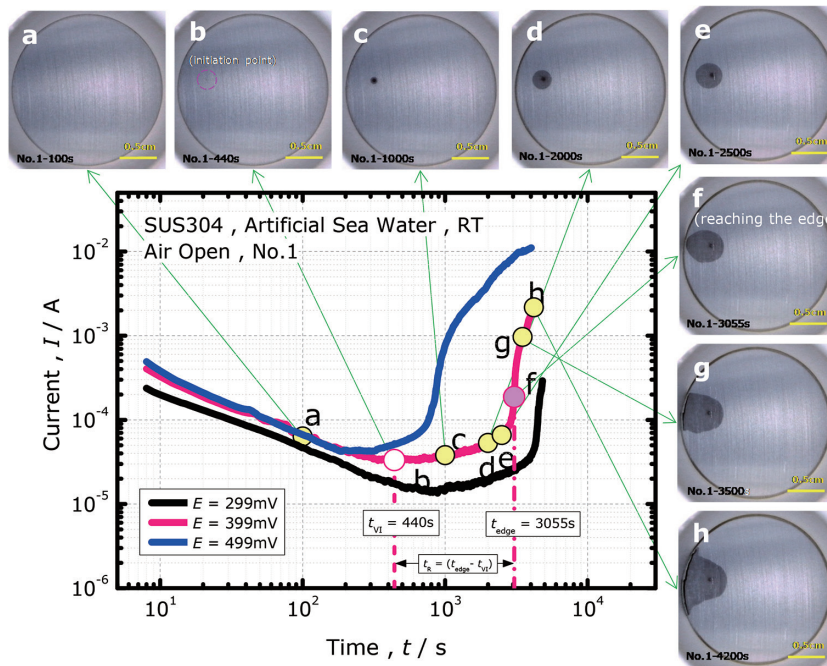


Fig. 19 Current-time curves and appearance change of inner crevice during potentiostat tests of SUS304 in artificial sea water

essary to control the oxidation behavior in the brazing atmosphere.<sup>58)</sup> The establishment of an in-situ observation method has clarified the effect of trace Al used as a deoxidizing element on the wetting and spreading behaviors of the braze during the heat treatment of brazed joints. As the Al content decreases, the Ni braze starts to wet and spread at a low temperature and provides good brazeability. It is clear that the oxide film formation, oxide film removal, and base metal melting behavior are related to the wetting and spreading of the braze.<sup>59)</sup> We hope to clarify the effects of the above-mentioned controlling factors and apply the findings to future solution technology.

#### 4. Future Prospects

To respond to environmentally-conscious resource conservation and new energy development in the future society, we must accurately grasp the needs and promote our research toward the functional enhancement of stainless steel. For this purpose, it is important to establish new development guidelines based on basic technology and efficiently combine them. In this chapter, we describe our initiatives for basic technology and its deployment.

#### 4.1 Initiatives for new corrosion control technology

The prime feature of stainless steel is corrosion resistance. The main corrosion form is local corrosion such as crevice corrosion and pitting corrosion. Here, we introduce our initiatives to elucidate the mechanism of crevice corrosion, and our utilization of exposure verification data for the optimum selection of stainless steel to suit specific locations of use.

##### 4.1.1 Elucidating mechanism of crevice corrosion and new initiatives

To understand crevice corrosion, a major issue with the corrosion resistance of stainless steel, we investigated the crevice corrosion propagation behavior in artificial seawater by the potentiostatic method. As shown in Fig. 19, crevice corrosion consists of the following steps: (i) Corrosion occurs in a crevice where the current initially drops; (ii) As the current gradually increases after the occurrence of corrosion, the corroded region circularly expands; and (iii) After reaching below the edge of the crevice, the corrosion proceeds and the current suddenly increases. The elementary steps of crevice corrosion initiation and propagation have been elucidated.<sup>60)</sup> The numerical analysis by the FEM of the potential and current density distributions inside and outside the crevices enables us to discuss

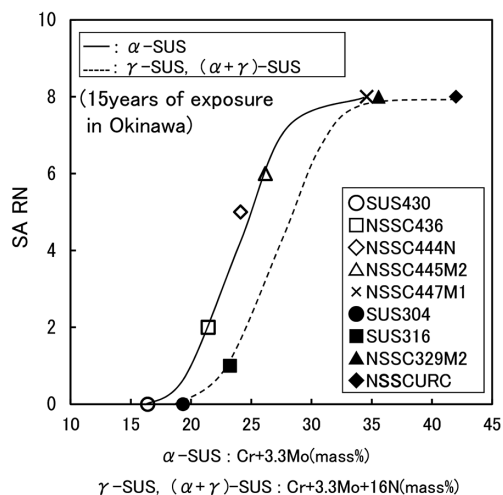


Fig. 20 Relation between rating number SARN and pitting index (Cr+3.3Mo+16N) after 15 years atmospheric exposure test in Okinawa

the potential disnoblement of the corrosion-initiated region and the change in the current density, and the drop in pH due to the elution of metal ions in front of the corrosion tip at the crevice edge side, and the corrosion propagation behavior, among other phenomena.<sup>61)</sup> Most recently, the relationship between the potential ennoblement phenomenon caused by microorganisms and the crevice corrosion has been clarified.<sup>62)</sup> The above basic research is expected to be applied to new corrosion control guidelines and material selection technology.

#### 4.1.2 Databasing and evolution of atmospheric corrosion data

In addition to the elucidation of phenomena such as crevice corrosion described above, we have investigated the weatherability of various stainless steels in actual environments for a long period. According to 15 years of exposure test results in a coastal environment in Okinawa, as shown in Fig. 20, red rust occurs in SUS304 and SUS316 and the rating number SARN is less than 1, whereas NSSC 445M2, NSSC 447M1 (30Cr-2Mo), NSSC 329M2 (25Cr-6.5Ni-3Mo-0.14N), and NSSC URC (25Cr-25Ni-5Mo-0.13N), as their pitting index (Cr+3.3Mo+16N) is greater than 26, show SARNs greater than 6 and almost no occurrence of red rust. Corrosion results were also found to differ with exposure locations (coastal, urban, or industrial).<sup>63)</sup> Concerning these results, laboratory cyclic corrosion tests showed that the corrosion depth is correlated with the salt deposit<sup>64)</sup> and that the initiation and propagation of pitting corrosion are greatly affected by the drying process of solution droplets.<sup>65)</sup> In the future, it will be important to quantitatively understand the effects of materials and environmental factors that affect corrosion initiation and propagation in the atmospheric environment, and to clarify suppression methods based on this understanding. In addition, it is expected that the development of optimal materials for not only the atmospheric environment but also the river environment and the life prediction corresponding to life cycle assessment (LCA) will be developed.

#### 4.2 Initiatives for new microstructure control technology

As another initiative to improve the properties of stainless steel, we have investigated the possibility of microstructure control as related to grain boundary control. Regarding the creep properties of austenitic stainless steel at high temperature for a long time, a grain boundary engineered material (GBEM) with an increased ratio of

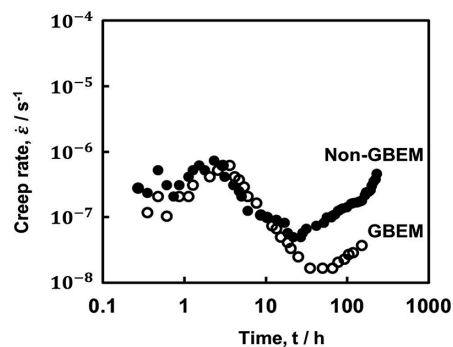


Fig. 21 Creep rates vs time curves for non-grain boundary engineered and grain boundary engineered SUSXM15J1 under stress of 96 MPa at 700°C

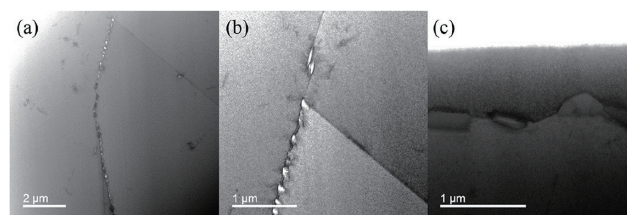


Fig. 22 Precipitates in grain boundary of SUSXM15J1 with 0.2% nitrogen after annealing at 900°C for 20 minutes BF-STEM images

coincidence grain boundaries has been found to have a longer transition of accelerated creep initiation time and a lower minimum creep rate than that of Non-GBEM in Fig. 21.<sup>66)</sup> In addition, the N is an inexpensive but effective high-temperature strengthening element. The N precipitates change in size and shape with grain boundaries as shown in Fig. 22.<sup>67)</sup> It may be utilized in both solid solutions and precipitates and may be combined with grain boundary control technology. The evolution of these findings into new microstructure control technology is expected.

Regarding duplex stainless steel, we have introduced the research and development of duplex stainless steel containing 20% or more Cr and having ferrite and austenite as the main phases. It is possible to manufacture a duplex stainless steel composed of martensite and retained austenite in a Cr range lower than that of the above-mentioned duplex stainless steel. A stainless steel with a strength of 1400 MPa class and a ductility of 20% or more is now under study<sup>68)</sup> and is expected to be applied in fields where strength and weight reduction are required.

In the development of new stainless steels, including those described above, it is even more necessary to establish guidelines for the control of internal and surface microstructures that maximize the properties, and to quantify the internal and surface microstructures. In terms of manufacturing technology, we must model the metallurgical phenomena occurring in the refining, solidification, hot rolling, cold rolling, and annealing processes and improve the efficiency of these processes. Another major research and development issue is the processing technology of the product and change in its properties during use.

## 5. Conclusions

To enhance the corrosion resistance, heat resistance, strength, and other properties of stainless steel, it is important to rationally utilize its many characteristic alloying elements and to control its microstructures. For that purpose, it is essential to understand the

microstructural changes of stainless steels in manufacture and use, to predict their microstructures throughout the processes, and to feedback the achieved results to manufacturing technology. The above-mentioned research and development activities must be efficiently carried out while grasping changing social needs. We will continue our research and development efforts to create more attractive stainless steels that can contribute to our future society.

### References

- 1) Oikawa, Y. et al.: J. Jpn. Weld. Soc. 82 (6), 435 (2013)
- 2) Oikawa, Y. et al.: CAMP-ISIJ. 33, 227 (2020)
- 3) Okada N. et al.: CAMP-ISIJ. 33, 228 (2020)
- 4) Blom, K. J.: Proc. Int. Conf. Stainless Steels '87, York, 1987
- 5) Oikawa, Y. et al.: CAMP-ISIJ. 24, 406 (2011)
- 6) Oikawa, Y. et al.: Materia Japan. 56 (10), 608 (2017)
- 7) Oikawa, Y. et al.: Stainless Steel World 2011 Conference & Exhibition, Maastricht, 2011
- 8) Oikawa, Y. et al.: CAMP-ISIJ. 24, 978 (2011)
- 9) Hatano, M.: Materia Japan. 54 (7), 356 (2015)
- 10) Matsuyama, H. et al.: CAMP-ISIJ. 24, 404 (2011)
- 11) Hiraide, N. et al.: 59th Japan Conference on Materials and Environments, D-203, (2012)
- 12) Hatano, M. et al.: Report on the Industrial Application Proposals at SPring-8. B1773BL46XU (2011)
- 13) Hamada, J. et al.: Materia Japan. 56 (1), 13 (2017)
- 14) Tomita, T. et al.: Nisshin Steel Technical Report. (90), 30 (2009)
- 15) Fujimura, Y. et al.: Nippon Seitetsu Giho. (416), 76 (2020)
- 16) Kanno, N. et al.: Tetsu-to-Hagané. 103 (9), 539 (2017)
- 17) Hiraide, N. et al.: Proceedings of JSAE Autumn Convention, 2016, p.367
- 18) Hiraide, N. et al.: Zairyo-to-Kankyo. 58, 20 (2009)
- 19) Kumano, N. et al.: CAMP-ISIJ. 25, 1251 (2012)
- 20) Kumano S. et al.: Nisshin Steel Technical Report. (98), 1 (2017)
- 21) Nonomura, A. et al.: Nisshin Steel Technical Report. (90), 20 (2009)
- 22) Matsushashi, T. et al.: Nippon Seitetsu Giho. (416), 52 (2020)
- 23) Fujimura, Y. et al.: CAMP-ISIJ. 30, 969 (2017)
- 24) Sugeoi, M. et al.: CAMP-ISIJ. 32, 711 (2019)
- 25) Yamasaki, S. et al.: Proc. of THERMEC '2016, Austria, 2016
- 26) Yamasaki, S. et al.: CAMP-ISIJ. 31, 850 (2018)
- 27) NEDO: Hydrogen Energy White Paper. 2015  
<http://www.nedo.go.jp/content/100567362.pdf>
- 28) Hatano, M. et al.: Journal of Fuel Cell Technology. 12 (4), 70 (2013)
- 29) Matsumoto, K. et al.: Tetsu-to-Hagané. 103 (1), 54 (2017)
- 30) Nagumo, M.: Fundamentals of Hydrogen Embrittlement. Uchida Rokakuho, 2008, p.1, 299
- 31) Hatano, M. et al.: Philosophical Magazine Letters. 99, 404 (2019)
- 32) Hatano, M. et al.: Symposium Proceedings of the Fundamental Factors and Practical Issues of Hydrogen Embrittlement, Japan Iron and Steel Institute, 2017
- 33) Hatano, M. et al.: Acta Materialia. 67, 342 (2014)
- 34) Sato, Y. et al.: Boshoku-Gijutu. 31, 319 (1982)
- 35) Yoshimi, T. et al.: Proceedings of the 26th Annual Conference on Ozone Science and Technology in Japan, Japan Ozone Association, 2017
- 36) JIS B 9946 Ozone Treatment Apparatus for Water and Wastewater Including Other Oxidation Uses—Specifications of Apparatus and Measurement Methods for Ozone Concentration
- 37) Yoshimi, T. et al.: Proceedings of the 24th Annual Conference on Ozone Science and Technology in Japan, Japan Ozone Association, 2015
- 38) Yoshimi, T. et al.: Proceedings of the 27th Annual Conference on Ozone Science and Technology in Japan, Japan Ozone Association, 2018
- 39) Okada, N. et al.: Zairyo-to-Kankyo. 66, 263 (2017)
- 40) Imai, M. et al.: Prestressed Concrete. 62 (1), 47 (2020)
- 41) Fukumoto, S. et al.: J. Japan Inst. Met. Mater. 73 (7), 502 (2009)
- 42) Fukumoto, S. et al.: Q. J. Jpn. Weld. Soc. 29 (3), 197 (2011)
- 43) Fukumoto, S. et al.: ISIJ International. 50 (3), 445 (2010)
- 44) Fukumoto, S. et al.: Welding Letters. 37 (4), 7 (2019)
- 45) Fukumoto, S. et al.: Tetsu-to-Hagané. 98 (7), 351 (2012)
- 46) Kimura, K. et al.: Tetsu-to-Hagané. 98 (11), 601 (2012)
- 47) Shibata, T. et al.: Nisshin Steel Technical Report. (99), 10 (2018)
- 48) Hamada, J. et al.: Materials Transactions. 50 (4), 752 (2009)
- 49) Nishimura, W. et al.: CAMP-ISIJ. 28, 839 (2015)
- 50) Mizoguchi, T. et al.: Nisshin Steel Technical Report. (97), 1 (2016)
- 51) Kawano, A. et al.: Nisshin Steel Technical Report. (97), 8 (2016)
- 52) Ishimaru, E.: ESI Users' Forum Japan, PUCA 2016, SF06
- 53) Kawa, M. et al.: CAMP-ISIJ. 30, 971 (2017)
- 54) Fukumoto, S. et al.: Q. J. Jpn. Weld. Soc. 37 (1), 1 (2019)
- 55) Yoshioka, Y. et al.: Q. J. Jpn. Weld. Soc. 37 (4), 133 (2019)
- 56) Iwasaki, Y. et al.: Q. J. Jpn. Weld. Soc. 37 (1), 24 (2019)
- 57) Yoshioka, Y. et al.: Preprints of the National Meeting of JWS, 105, 56 (2019)
- 58) Mizoguchi, T. et al.: CAMP-ISIJ. 24, 977 (2011)
- 59) Hayashi, A. et al.: Nippon Seitetsu Giho. (416), 101 (2020)
- 60) Matsushashi, R. et al.: Zairyo-to-Kankyo. 64, 51 (2015)
- 61) Matsuoka, K. et al.: Zairyo-to-Kankyo. 65, 350 (2016)
- 62) Nose, K. et al.: Proceedings of the 185th Symposium on Corrosion Engineering, 11 (2016)
- 63) Shiotsuki K. et al.: Nisshin Steel Technical Report. (91), 25 (2010)
- 64) Mizoguchi, T. et al.: 60th Japan Conference on Materials and Environments, 191 (2013)
- 65) Sampei, S. et al.: CAMP-ISIJ. 30, 1271 (2017)
- 66) Ikeda, N. et al.: CAMP-ISIJ. 31, 812 (2018)
- 67) Ochi, M. et al.: Tetsu-to-Hagané. 105 (4), 418 (2019)
- 68) Hirakawa, N. et al.: Nippon Seitetsu Giho. (416), 107 (2020)



Masayuki ABE  
Executive Officer  
Head of Research & Development Center  
Research & Development Center  
Nippon Steel Stainless Steel Corporation  
3434 Ooaza-shimata, Hikari City, Yamaguchi Pref. 743-8550